Fabricating Hollow 3D Microstructures in Glass

Myra Kurosu Jalil and Rajorshi Paul
Mentors: Swaroop Kommera, Antonio Ricco and Maurice Stevens

1. Introduction

1.1 Motivation

Microfluidic devices are tools that allow for fluid flow in small (~μm-mm sized) channels, which makes them useful for manipulating or performing chemical reactions with small volumes of reagents, or for applications that involve manipulating or observing small objects, such as single cells or small pieces of tissue. Microfluidic devices are used by researchers to perform a wide range of processes and experiments, and are typically fabricated in polydimethylsiloxane (PDMS) using soft lithography techniques. First, a master mold is fabricated using photolithography by selectively curing photoresist on a silicon wafer to form patterns that constitute the channels of a microfluidic device. Next, the patterns are transferred onto a layer of PDMS, and bonded to a clean substrate to form enclosed channels in which fluids can flow.

While the PDMS-based fabrication process has a lot of advantages, such as the ability to make multiple copies of the microfluidic device from one master mold and quick fabrication turnaround, PDMS devices suffer from a few drawbacks. First, it is difficult to fabricate complex 3D microstructures. Most 3D microfluidic devices rely on curing multiple layers of photoresist, or stacking up layers of patterned PDMS on top of each other. While it is possible to fabricate 3D microstructures using rapid prototyping tools on the nano- and micron scale, like the Nanoscribe, there are design limitations as the mold must allow for PDMS to be peeled off the mold without destroying the pattern (i.e., there cannot be any overhanging patterns on the mold). Second, PDMS is soft and prone to deforming under high pressure during device operation. Therefore, it is difficult to control the pressure distribution inside the microfluidic channel. Third, debris build-up inside microfluidic channels during operation is often irreversible, and can lead to the need to frequently replace microfluidic devices. For these reasons, PDMS is not a preferred choice for fabricating microfluidic channels both at the industrial scale, and in the academic setting.

Glass is a good alternative material for microfluidic device fabrication. Glass, with its greater compatibility with solvents, high pressure and high temperature than PDMS, addresses all of the aforementioned drawbacks. First, using the process proposed in this work, it would be straightforward to embed templates of any shape into a silica glass structure to form microfluidic devices with complex 3D geometries. Second, unlike PDMS, glass does not deform under the magnitude of pressures that fall within the operating ranges of most microfluidic devices (up to ~kPa). Third, debris build-up in glass devices can be removed by heat treatment, which would allow for glass devices to be reused.

1.2 Proposed process

Recently, Kotz et al. demonstrated a novel technique for embedding hollow 3D microstructures in glass (**Fig. 1**). [1] First, they embedded a sacrificial 3D template inside a slab of silica nanocomposite. The silica nanocomposite was prepared by dispersing 40% hydrophilic fumed silica nanoparticles (Aerosil OX 50, Evonik) in a solution of binding agents and a photoinitiator. The template was transferred to the nanocomposite by pouring the nanocomposite over the 3D template, UV curing the nanocomposite, and finally peeling

off the embedded template from the substrate. The process was repeated after flipping the cured composite over so that the entire template was fully embedded inside the cured nanocomposite. The next step was to thermally debind the cured nanocomposite at 600℃ to remove the binding agents. This process also oxidized the material of the template to leave behind a hollow 3D microstructure embedded inside a slab of silica particles. Finally, the slab was sintered at 1300℃ under a pressure of 5×10^{-2} mbar inside a vacuum furnace to densify the silica particles, thereby creating transparent fused silica glass with an embedded hollow 3D microchannel. There was a reported linear shrinkage of 26.3% during the sintering process.

In this project, we developed a process flow for fabricating 3D microstructures inside glass by adapting the work done by Kotz et al. Our goal was to make the process more accessible to SNF and SNSF users by using equipment that are readily available at the SNF.

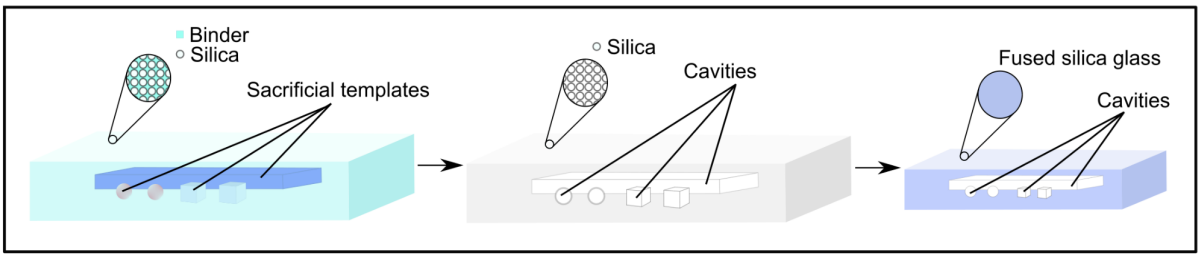

Figure 1. The process flow for fabricating hollow structures within transparent fused silica glass. [1] First, a sacrificial template is embedded into a nanocomposite consisting of silica particles and binding agents. The nanocomposite is solidified by UV curing. Second, the cured nanocomposite undergoes thermal debinding to remove the binding agents and the sacrificial templates. Third, the silica structure was sintered to densify the silica nanoparticles and produce a transparent fused silica glass structure embedded with hollow cavities.

1.3 Benefits to SNF and SNSF community

We developed a standard operating procedure (SOP) for the fabrication of hollow structures in transparent glass using equipment available at the SNF or other facilities on the Stanford campus. In the SOP, in addition to detailing the process for fabricating transparent glass, we highlight and address safety considerations as they relate to working with silica nanoparticles, and we provide tips on troubleshooting potential issues.

Current methods for producing 3D microchannels require complex multistep processes or outsourcing to companies. This SOP will allow users to fabricate complex hollow 3D nano- and micro- sized features in glass more easily and in-house. The proposed process flow is relatively new to the microfluidics community and, therefore, standardizing this process at the SNF will enable users who use microfluidics as an essential tool to fabricate complex 3D geometries faster and at a lower cost. An in-house process will allow users to perform more experiments than if fabrication were outsourced, and users can explore new applications of hollow cavities embedded in glass.

2. Methods

2.1 Template fabrication

We designed the 3D sacrificial templates for the hollow structures in SolidWorks 2020 (Dassault Systèmes) and printed them using high-resolution two-photon polymerization on the Nanoscribe Photonic Professional GT tool.

When designing the template (**Fig. 2**), we wanted to explore the different shapes, dimensions, and aspect ratios that we could replicate in glass, and we wanted to keep the shapes relatively simple. Our test template consisted of spheres, cubes, and two long rectangular prisms designed to imitate the straight channels that are commonly used in microfluidic devices. The dimensions of the features were chosen to be similar to those of some of the microfluidic devices we have previously used, assuming that there would be linear shrinkage of ~30%.

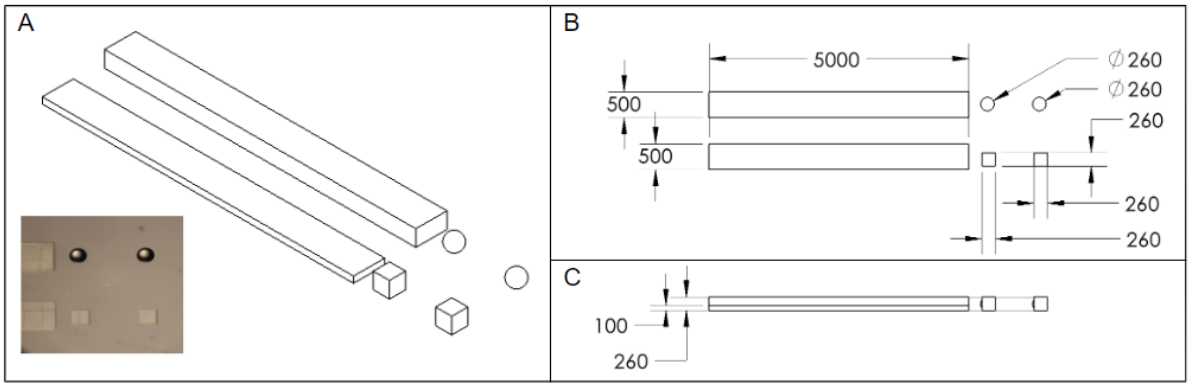

Figure 2. A photograph and drawings of the template we embedded in the silica nanocomposite. **A.** An isometric view of the template design. The inset shows a photograph taken of a small region of the template after printing and development. **B.** A top view of the template design, showing the widths and lengths of the long channels and cubes, and the diameters of the spheres. **C.** A front view of the template design, showing the heights of all features. One channel is smaller in height than the other (100 µm vs. 260 µm). All dimensions are in µm.

We generated an STL file of the model in SolidWorks and used DeScribe 2.7 (Nanoscribe) to convert the STL to a script in Nanoscribe's General Writing Language (GWL) using the default recipe for printing in IP-S resist using a 25x objective in shell-and-scaffold mode. The GWL job file was then imported into the NanoWrite software (Nanoscribe), which we used to control the Photonic Professional GT system and load the job to be printed.

We used the 25x objective lens to print the templates in IP-S resist on a clean ITO coated glass slide in the dip-in laser lithography configuration. We followed the instructions in the Photonic Professional GT user manual, which can be found on the SNF equipment page for the Nanoscribe tool. The print job took over 6 hours to complete. We developed the IP-S print in SU-8 Developer and isopropanol following the instructions in the manual, and we inspected the template on the Keyence Digital Microscope VHX-6000.

2.2 Nanocomposite preparation

The nanocomposite is made of silica nanoparticles (NPs) dispersed in a solution of binding agents and a photoinitiator. We prepared the nanocomposite by adapting the protocol in Kotz et al.[1] Briefly, we prepared a 60 mL solution of the binding agents containing 68% v/v 2-hydroxyethyl methacrylate (40.8 mL, cat no. AAB2426022, Thermo Fisher Scientific), 7% v/v tetra(ethylene glycol) diacrylate (4.2 mL, cat. no. 398802, Sigma-Aldrich), and 25% v/v 2-phenoxyethanol (15 mL, cat. no. 77699, Sigma-Aldrich) in a 500 mL glass beaker inside a fume hood.

The next step was to disperse the hydrophilic silica NPs (Aerosil OX 50, Evonik) into the solution of binding agents. Since repeated exposure to silica NPs can be harmful, we performed all steps involving the handling of dry silica NPs in a sealed glove bag placed inside a fume hood, and while wearing N95 (or equivalent) respirators. The silica NPs were provided to us in containers that were too large to fit into the glove bags available to us, so we cut open a large glove bag and sealed it around the container of silica NPs. Working inside the glove bag, we aliquoted ~5 g of silica NPs into eighteen 50 mL conical tubes to obtain a total of ~90 g silica NPs. We removed as much residual silica NPs from the outside of the tubes as possible, and then transferred them to a second glove bag containing the solution of binding agents for dispersion.

To disperse 88 g of the silica NPs into the binding agent solution (and obtain a 40% v/v dispersion of silica NPs in 100 mL nanocomposite), we first tried to use a magnetic stirrer while slowly adding small amounts of the silica NPs, but found the dispersion to be time-consuming and difficult as the silica content increased due to the increasing viscosity of the fluid. We then tried using a handheld immersion blender, which worked very well to disperse the NPs. For the first ~35 g, we were able to disperse the silica NPs by swirling the beaker, without using the immersion blender. Once the dispersion became relatively viscous, we alternated between pouring two 5 g silica NP tubes into the beaker, “folding” it into the dispersion using a spatula, and running the immersion blender for 30 seconds until all ~88 g of the silica NPs had been dispersed. During the operation of the immersion blender, we noticed that the temperature of the dispersion increased, likely due to friction with the blades. This added heat likely reduced the viscosity of the dispersion, making it easier to mix in additional silica NPs. Finally, we scraped the sides of the beaker and the tip of the immersion blender and ran the immersion blender for 1-2 minutes to ensure that all of the available silica NPs were fully dispersed. The dispersion process using the immersion blender took ~1 hour.

We poured the dispersion into 10 mL aliquots in 50 mL conical tubes. We then added 0.5% w/v of the photoinitiator 2,2-dimethoxy-2-phenylacetophenone (50 mg in 10 mL dispersion, cat. no. 196118, Sigma-Aldrich). Finally, to complete the preparation of the nanocomposite, we sonicated the dispersion for 15 minutes to mix in the photoinitiator, and we removed air bubbles from the dispersion under vacuum in a desiccator for 1-2 hours, using aluminum foil to protect it from light.

2.3 Template embedding and nanocomposite curing

We optimized the final protocol to embed the template in the nanocomposite in multiple stages. In the first method we tried (**Fig. 3**), we made rectangular molds out of PDMS (Sylgard 182, Dow Corning) by mixing the base and curing agent in a 10:1 ratio, pouring it into a 100 mm petri dish, and curing it at 65℃ for at least 4 hours to form a thick, solid PDMS slab from which we cut out a rectangular section. We placed the PDMS mold over the glass slide with the template to contain the liquid nanocomposite before curing it with a UV lamp (365 nm) for 4 minutes. Then we carefully peeled the solid nanocomposite (including the embedded template) off the glass slide, flipped it over so that the embedded template was facing up, and repeated the process to cure another layer of nanocomposite and fully enclose the template within a solid piece of cured nanocomposite. We did not control the thickness of the nanocomposite layers, and the resulting structure was ~1 cm thick.

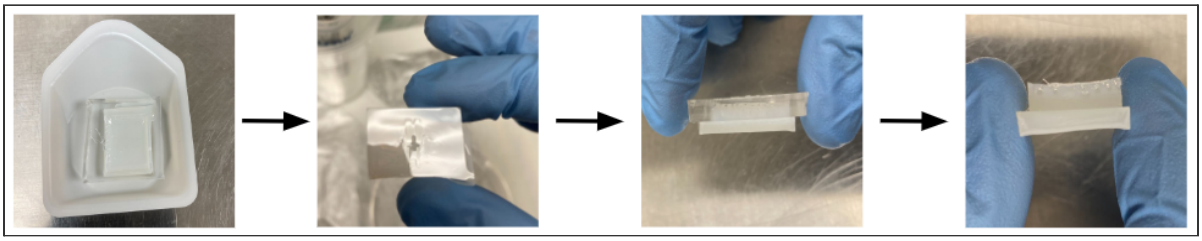

Figure 3. The first method we used for template embedding. First, we cured a layer of nanocomposite over the template on the glass slide. Second, we peeled the cured nanocomposite off the glass slide, leaving behind only some residue of IP-S resist on the glass slide. Third, we cured a second layer of nanocomposite over the exposed region of the template. Finally, we are left with a solid piece of nanocomposite containing the embedded template.

After debinding and sintering these samples of cured nanocomposite, we found that the rectangular mold shape was not optimal due to the stress concentrations formed at the corners of the rectangles (this is discussed in detail in section 3.1), and that the samples were too thick (also discussed in section 3.1). Therefore, we made circular molds instead using a 9/16” hole punch from a 2 mm slab of PDMS (**Fig. 4**). All of the other steps remained the same.

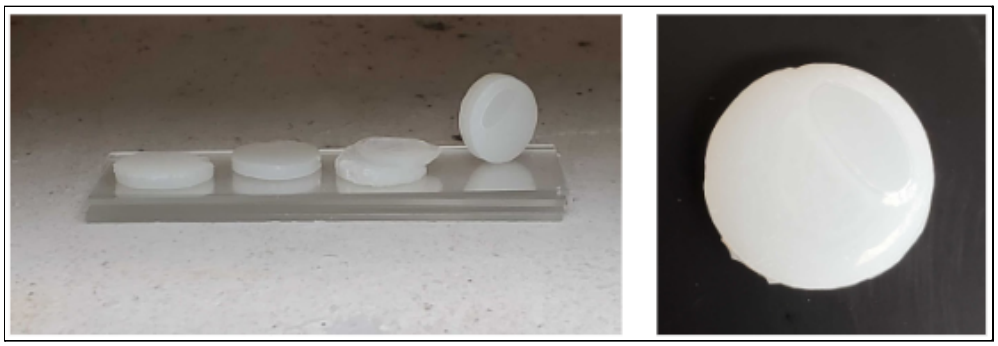

Figure 4. Cured nanocomposite samples made using the 9/16” circular molds.

It was found that the 2 mm nanocomposite samples were still too thick and continued to cause issues in downstream processes, so we updated the template embedding process (**Fig.**

5) to be able to produce samples that were 600 µm thick (we found that this was the lower limit, as samples thinner than 600 µm were difficult to make).

We made 600 µm thick layers of PDMS in a process similar to that used to make the thicker PDMS slabs, except that we only needed to heat the PDMS for 15 minutes at 100℃ for it to fully cure. We used the 9/16" hole punch to make the mold. Because we predicted that 600 µm thick pieces of nanocomposite would be very difficult to remove from the glass slide after curing the first layer, we covered most of the glass slide (except the template) with Scotch tape to allow for easier separation of the glass slide from the nanocomposite. We placed the 600 µm PDMS mold over the glass slide to form a well to contain the liquid nanocomposite. We used a wooden stick to drop a small volume of the nanocomposite into the well, and covered it with a thick slab of PDMS, gently pressing down to remove any excess nanocomposite and air bubbles. We cured the nanocomposite under 365 nm UV light for 4 minutes. We then peeled the tape off the glass slide, with the nanocomposite sitting on top of the tape. The tape was difficult to peel off the nanocomposite sample, so we used a scalpel blade to gently scrape it off the sample. After removing all traces of the tape, we flipped over the cured nanocomposite and applied a very thin layer of liquid nanocomposite over the exposed template. We used a thick PDMS slab to flatten the liquid nanocomposite and UV cured it for 4 minutes, finally producing a fully cured nanocomposite sample that was a little thicker than 600 µm (closer to 750-800 µm with some variability). This is our final, and most successful, process for embedding the template in cured nanocomposite.

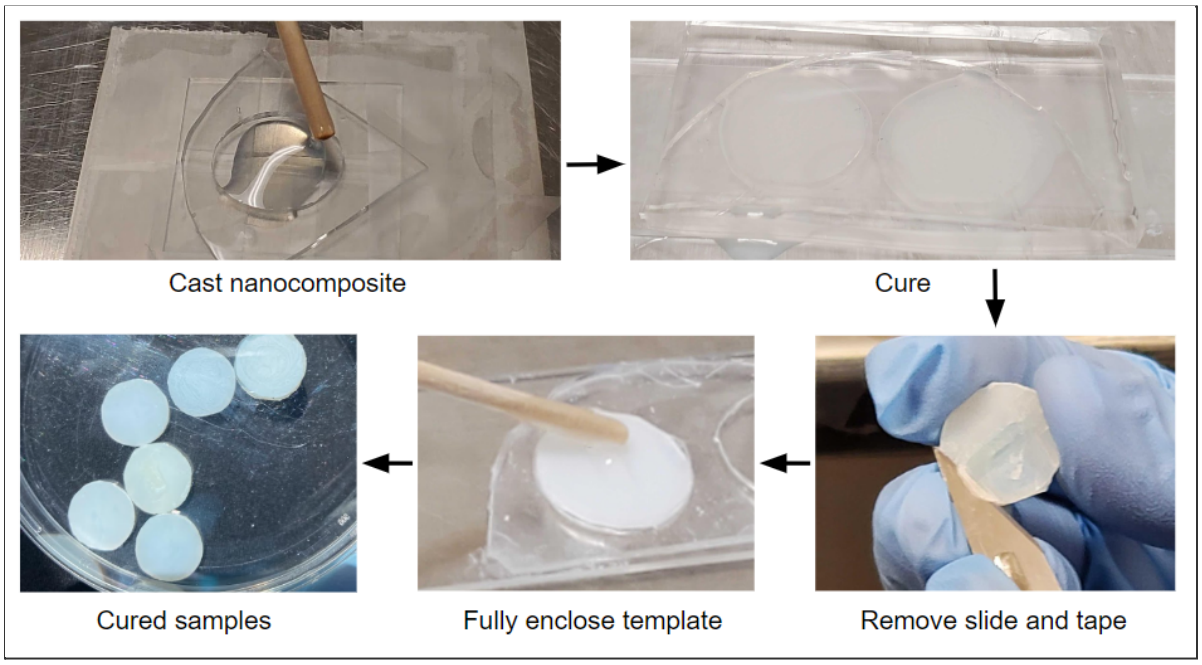

Figure 5. The final method for embedding the IP-S template in cured nanocomposite.

During all of our experiments, we also prepared some samples of cured nanocomposite without the template. Most samples without templates were made of only one layer of nanocomposite, but some were made of two layers and were prepared in the same way a sample with the template would have been prepared. This allowed us to compare the

outcomes of samples that had different thicknesses, and have replicates of the samples in each round of debinding and sintering.

2.4 Debinding

We tried three processes for thermally debinding the solid nanocomposite samples, which are summarized in the tables below. We tried the debinding step in two furnaces, the Thermolyne at the SNF and the Lindberg BlueM furnace at the Uytengsu Teaching Laboratory in Shriram (UTL). Out of these, the Thermolyne is programmable up to 8 steps, while the Lindberg BlueM is not programmable. We programmed the thermolyne following the instructions in the operation manual for the thermolyne 48000 furnace. [2]

Table 1. Thermal debinding following the published protocol in Thermolyne with controlled ramp rate, in air.

Temperature (℃)	Ramp rate (℃/min)	Holding duration (hh:mm)
150	0.5	02:00
320	0.5	04:00
600	0.5	02:00
25	5	N/A

Table 2. Thermal debinding variation 1 in Lindberg BlueM furnace with uncontrolled ramp rate (1-10℃/min), in air.

Temperature (℃)	Ramp rate (℃/min)	Holding duration (hh:mm)
150	N/A	06:30
320	N/A	12:00
450	N/A	04:30
600	N/A	06:00
25	N/A	N/A

Table 3. Thermal debinding variation 2 in Lindberg BlueM furnace with uncontrolled ramp rate (1-10℃/min), in air.

Temperature (℃)	Ramp rate (℃/min)	Holding duration (hh:mm)
150	N/A	04:30
320	N/A	10:00

450	N/A	03:00
600	N/A	04:00
25	N/A	N/A

We found that all three processes for debinding had similar outcomes, except that the samples that underwent debinding without controlled ramping seemed slightly more prone to breaking and cracking. However, we had simultaneously reduced the thickness of the samples, so we cannot attribute the increased fragility of the samples solely to the uncontrolled ramp rate during debinding. In general, the samples were very brittle after debinding and had to be handled with care. No warping or deformation occurred during debinding (**Fig. 6**). Additionally, since all three processes worked well, we tentatively concluded that a low ramping rate is not critical during debinding for these samples, and that the holding temperature and durations can be modified with some leeway, as long as the total debinding time and the holding time at 600℃ are maintained at >20 hours and >2 hours, respectively.

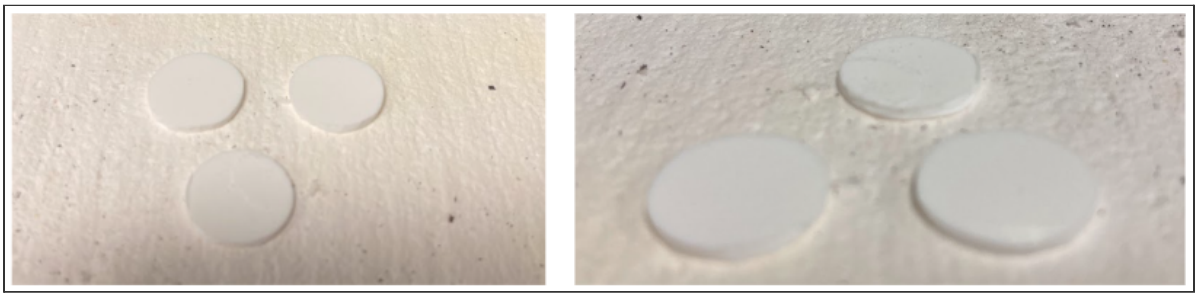

Figure 6. Photographs of the samples after thermal debinding, during which the binding agents and IP-S template are removed from the bulk silica.

2.5 Sintering

We tried four processes for sintering the samples, which are summarized in the tables below. We sintered the glass in three furnaces, tylan9 (SNF), Thermolyne (SNF) and the Lindberg BlueM furnace (UTL). Out of these, the first two furnaces are programmable, and the third furnace is non-programmable. However, out of the three, only the Thermolyne could be programmed to operate at a set ramp rate. We did not have the ability to control the pressure in any of the furnaces, and the maximum operating temperature of all three furnaces was either 1100℃ (tylan9 and Lindberg BlueM) or 1200℃ (Thermolyne). We did have the ability to sinter the samples under nitrogen gas in the tylan9 furnace.

Table 1. Process A: Sintering in Thermolyne using the published protocol with controlled ramp rate, in air.

Temperature (℃)	**Ramp rate (℃/min)**	**Holding duration (hh:mm)**
800	3	01:30

1180	3	02:00
25	3	N/A

Table 2. Process B: Sintering in tylan9 with uncontrolled ramp rate, multiple holding steps to maintain the same total sintering program time as the published protocol, and under N_2 gas.

Temperature (℃)	**Ramp rate (℃/min)**	**Holding duration (hh:mm)**
360	N/A	02:00
450	N/A	00:30
540	N/A	00:30
630	N/A	00:30
720	N/A	00:30
800	N/A	02:00
890	N/A	00:30
980	N/A	00:30
1100	N/A	02:40
980	N/A	00:40
900	N/A	00:30
810	N/A	00:30
720	N/A	00:30
630	N/A	00:30
540	N/A	00:30
450	N/A	00:30
360	N/A	00:30

Table 3. Process C: Sintering in Thermolyne using the published protocol with controlled ramp rate, in air and extending the sintering process in Lindberg BlueM furnace with uncontrolled ramp rate (1-10℃/min) in air, extending the total sintering time to 6+ days. Process C extended the sintering time for some of the samples that had previously been sintered in Process A.

Temperature (℃)	Ramp rate (℃/min)	Holding duration (hh:mm unless otherwise stated)
800	3	01:30
1180	3	02:00
25	3	N/A
1100	N/A	6 days

Table 4. Process D: Sintering in Lindberg BlueM furnace with uncontrolled ramp rate (1-10℃/min) in air, extending the sintering time to 9+ days.

Temperature (℃)	Ramp rate (℃/min)	Holding duration (hh:mm unless otherwise stated)
400	N/A	02:00
800	N/A	03:00
1100	N/A	9 days

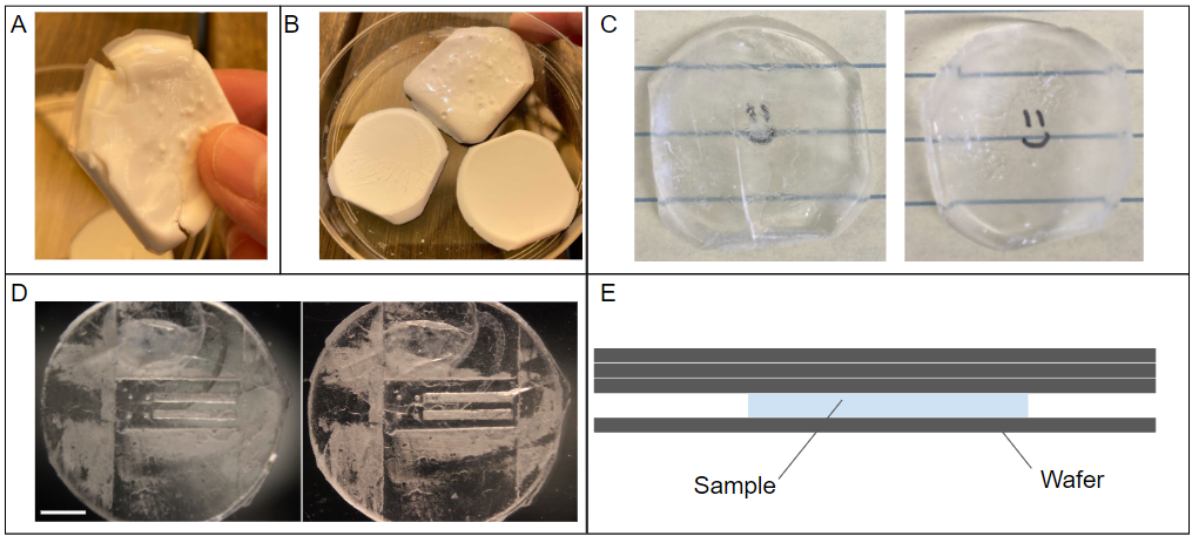

Figure 7. Photographs of the resulting silica glass samples during or after sintering. **A.** Glass after completing Process A. **B.** Glass after completing Process B. **C.** Glass during Process C, after glass has been at 1100℃ for 2 days (left). A different glass sample after completing Process C (right). **D.** Glass during Process D, after glass has been at 1100℃ for 4 days (left). The same glass sample after completing Process D (right). Scale bar is 2 mm **E.** During Process D, we sandwiched the silica samples between silicon wafers treated with kiln wash to reduce warping and deformation in the sample.

The key steps in the sintering process to obtain transparent glass with minimal deformation were 1) to extend the time for which the samples were held at 1100℃, and 2) to insulate the samples from the furnace floor. While sintering in Process D, the samples were placed on one wafer and covered with three wafers, with dried kiln wash coating the surfaces of the wafers that were in contact with the samples (**Fig. 7E**). This is discussed further in section 3.1. There is a limit to the effects of sintering; we found no difference in shrinkage or transparency for a sample held at 1100℃ for 4 days and 9 days (**Fig. 7D**). Additionally, it appears that sintering can be interrupted without any negative effects, as we observed that glass samples that were removed from the Thermolyne furnace for inspection continued to turn more transparent once sintering was resumed in the Lindberg BlueM (**Fig. 7A and 7C**).

3. Results and discussion

3.1 Crack formation and warping during sintering

After sintering some of the rectangular samples, we noticed that there was greater warping near the corners than other regions of the samples. To address this issue, we eliminated the stress concentrations caused by the presence of corners by curing all subsequent samples in circular molds.

Additionally, some of the thicker samples were cracked (**Fig. 7A**). We hypothesized that the cause of the cracking during sintering was a non-uniform heat distribution within the sample, which was quite thick (>> 2 mm). We therefore reduced the thickness of subsequent samples to help distribute the heat more evenly, which we hypothesized would help reduce warping and, therefore, crack formation.

The first round of sintering that produced transparent glass also resulted in significant warping of the glass sample, despite the reduced thickness of the glass sample (**Fig. 7C**, right). During this sintering process, we had placed the samples directly on the bottom surface of the furnace. As the conduction of heat through the surfaces of the furnace was faster than heat transfer through air, there was likely still a non-uniform heat distribution throughout the sample. We also noticed that the Lindberg BlueM furnace had hot spots where the heating effect was maximized, which led to issues of non-uniform heating between samples.

To minimize the issues caused by non-uniform heating within and between samples, we sandwiched the samples between silicon wafers: we placed the samples on one wafer and stacked three wafers on top of the samples. This helped insulate the samples from the bottom surface of the furnace and weighed down the samples. The combined effects of reducing the sample thickness, insulating the bottom surfaces of the samples, and weighing down the samples helped prevent warping of the samples during subsequent sintering processes (**Fig. 7D**). It is possible that a slower ramp rate during the sintering process would also help further reduce any warping effects.

3.2 Shrinkage

We found that the bulk silica experienced a linear shrinkage of ~21% during the sintering process (the diameter of the samples was reduced from ~1.4 cm to ~1.1 cm). This is similar to the linear shrinkage of 26.3% that Kotz et al. reported for a nanocomposite with 40% silica.

3.3 Transparency

We initially found it difficult to produce transparent glass after sintering. We had anticipated that we may run into this issue as the furnaces we had access to could not reach the ideal operating sintering temperature or pressure for the protocol that we were following. We did notice, however, that the edges of some of the samples were starting to turn translucent (**Fig. 7A**). Therefore, we reduced the thickness of the samples to allow for faster heat conduction into the middle of the sample, which we hypothesized would help speed up the sintering process. Additionally, we extended the sintering process to multiple days. The combined effects of these two changes allowed for the formation of relatively transparent glass (**Fig. 7C and 7D**).

3.4 Usability of hollow structures in glass as microfluidic channels

To test whether the channels formed in the glass sample could be used as parts of microfluidic devices, we flowed dye into a glass sample containing a long, straight channel by dipping one end of the open channel into a drop of dye and applying a vacuum. We were able to flow dye through the channel, without running into any obstructions (**Fig. 8**).

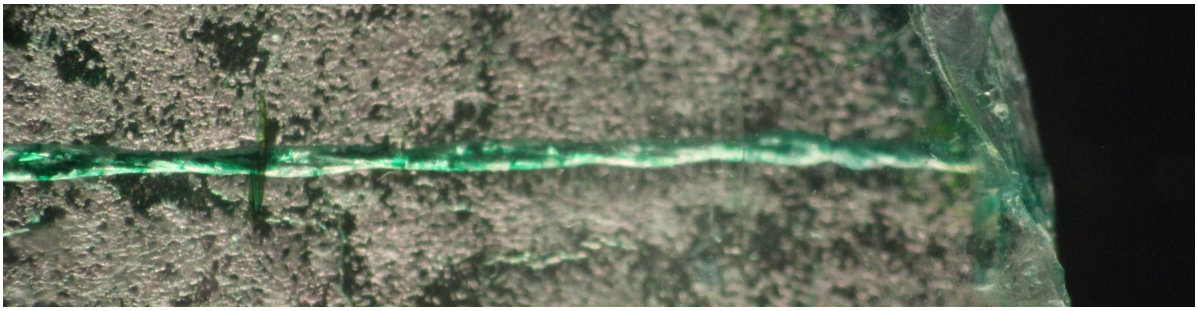

Figure 8. Flowing green dye into a channel that runs through the entire glass sample.

4. Conclusions and future directions

We have adapted a published protocol by Kotz et al. [1] to create an SOP for fabricating fused silica glass using the resources available at the SNF and UTL. We have created a safe and relatively easy process to fabricate microfluidic devices in glass that can be used by many research groups on campus, including ours, and can easily be adapted to any lab that has access to similar equipment. This procedure for embedding microstructures in glass is interesting and exciting because the possibilities are endless! Any template that will burn and be removed during thermal debinding should work, allowing for a wide variety of materials to be used to form the template.

Going forward, we plan to embed more complex 3D microstructures in glass to form microfluidic devices that can be used for some of our experiments. In order for the devices to be functional, we will need to build adapters to connect tubing to the devices to allow for fluid injection. Additionally, we would like to explore the effect of increased silica content in the nanocomposite on the transparency of the fused silica glass. We would also like to explore the cause of the opaque regions we commonly see on the surface of the sintered glass, which we suspect may be caused by defects in the photocured nanocomposite.

5. Budget

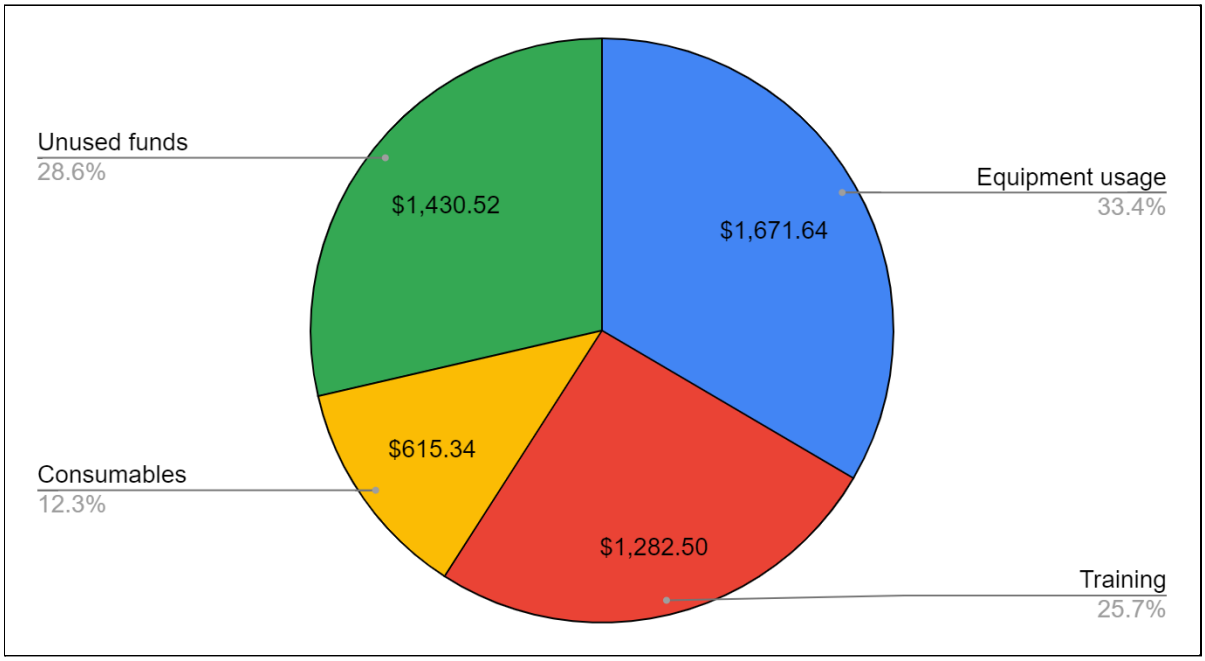

We were able to reduce the cost of equipment usage by using the furnaces at the UTL, which had no costs associated with usage. This was especially useful for sintering, which took multiple days to complete and would otherwise be a very expensive process. We were able to save 28.6% of the funds awarded to our project.

6. Acknowledgements

We would like to thank our mentors (Swaroop Kommera, Antonio Ricco and Maurice Stevens), the E241 instructor (Roger Howe) and teaching team, and the staff at the SNF for their support, invaluable guidance, and insights. We would also like to thank the staff at the Uytengsu Teaching Laboratory in Shriram (Jeffrey Tok and Mong Saetern) for providing us with a workspace, training, and access to the equipment at the UTL. We are grateful to Evonik for supplying us with Aerosil OX 50 silica nanoparticles.

7. References

1. Kotz, F. et al. Fabrication of arbitrary three-dimensional suspended hollow microstructures in transparent fused silica glass. Nat. Commun. 10, 1439 (2019).
2. Barnstead International. Type 47900 & 48000 Furnaces Operation Manual. (2002).